Macromolecules

ARTICLE

pubs.acs.org/Macromolecules

Hydrogen Bond Assisted Assembly of Well-Ordered Polyhedral Oligomeric Silsesquioxane−Block Copolymer Composites

Vikram K. Daga,[†] Eric R. Anderson,[‡] Samuel P. Gido,[‡] and James J. Watkins*[,‡]

[†]Department of Chemical Engineering and [‡]Department of Polymer Science and Engineering, University of Massachusetts Amherst, Amherst, Massachusetts 01003, United States

Supporting Information

ABSTRACT: Well-ordered block copolymer nanocomposites with *d*-spacings as small as 15 nm and additive loadings greater than 70 mass % were formed upon blending functionalized polyhedral oligomeric silsesquioxanes (POSS) additives into disordered block copolymers containing poly(ethylene oxide) (PEO) as one of the blocks. The POSS additives were functionalized with maleamic acid or aminophenyl groups as ligands to enable selective hydrogen bonding with the PEO chains. The selective interaction of the additives with the PEO chains caused microphase separation of the block copolymer leading to formation of well-ordered morphologies as evidenced by small-angle X-ray scattering. Further addition of the additive induced transitions between cylindrical and spherical morphologies. While both ligands induced order, the maleamic acid ligand enabled higher levels of incorporation of POSS cages into the PEO phases of the composite. Differential scanning calorimetry and wide-angle X-ray diffraction were performed to confirm compatibility and good mixing of the additives within the PEO phase. The maleamic ligands can be cross-linked by a thermal treatment. The cross-linking was used to stabilize the structure of the composites prior to calcination at high temperatures, which resulted in the formation of mesoporous silica. Transmission electron microscopy showed that the cylindrical and spherical morphologies of the parent composites were maintained in the mesoporous silica.

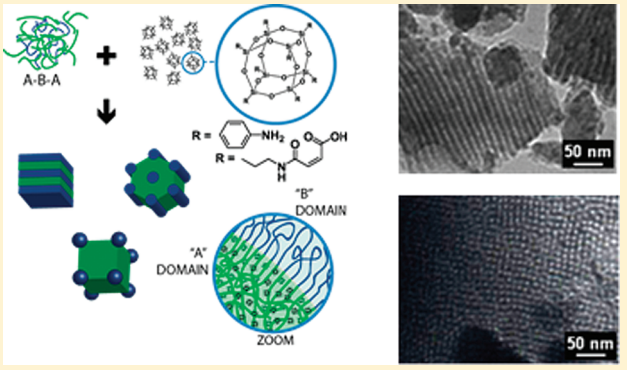

INTRODUCTION

Blends of nanoscale fillers and polymers are of interest for a wide range of applications. Among these, block copolymer (BCP) nanocomposites[1] are an interesting class of materials in which the block copolymer can guide the spatial location and periodic assembly of the additives.[2−4] This approach exploits differences between the chemical nature of the constituent blocks to direct the organization of additives, including small molecules, homopolymers and nanoparticles.[5−11] The selective incorporation of additives within one of the phases can create functional materials or enhance differences in the chemical and/or physical characteristics of the domains. In block copolymer lithography, for example, the etch resistance of one of the phases can be enhanced by selective incorporation of materials with high etch resistance.[12] BCP composites can also find use as low line edge roughness resists for nanoscale electronics[13] and as templates for the fabrication of nanoscale microelectronic structures, including high density data storage media.[14−16] A recent review summarizes the use of BCP nanostructures in electronics.[17] BCP composites materials are also of interest for photovoltaics[18−20] and photonics.[21−23] Other applications include their use as templates for the fabrication of inorganic mesostructured materials via phase selective reactions[24−26] or the formation of nanoporous polymeric materials by treating the BCP composites to remove the minority phase.[27−29] In some cases, the additives have been used to influence domain orientation.[30−33] Many applications and materials synthesis schemes would benefit from high concentrations of an additive within an ordered block copolymer composite, however entropic penalties associated with BCP chain stretching can severely limit additive loadings.[34] Recently Wiesner and co-workers demonstrated one specific example of a highly loaded and well-ordered polymer−nanoparticle assembly using strong interactions between ionic liquid ligands bound to the surface of Pt nanoparticles and a specially designed BCP.[35]

Microphase separation of BCPs is thermodynamically governed by the segregation strength between the chemically dissimilar blocks. A measure of segregation strength is provided by the product χN where χ is the Flory−Huggins interaction parameter between segments of the dissimilar blocks and N is the total number of repeat units. When the segregation strength is high, BCPs containing two chemically dissimilar blocks form spherical, cylindrical, or lamellar morphologies depending upon the relative volume fractions of the dissimilar blocks.[2,3] However,

Received: April 22, 2011
Revised: July 20, 2011
Published: August 10, 2011

when the critical segregation strength for microphase separation is not met, either due to a small χ and/or a small N, the BCPs remain disordered.[3,36,37] This is the case for the BCPs employed in this work. The segregation strength of disordered BCPs can be enhanced by blending selectively interacting additives. For example, blending of lithium[38−41] and gold[14,42] salts in PEO containing BCPs is known to enhance the segregation strength and induce ordering. One advantage of this approach is the formation of an ordered structure from low molecular weight BCPs, which can yield small domain sizes and d-spacings.[14] Recently we reported that selectively interacting homopolymers can be incorporated into otherwise disordered Pluronic BCPs at high loadings by utilizing hydrogen bonding interaction between the PEO blocks and the homopolymers. Although neat Pluronic BCPs are disordered in the melt due to low segregation strength, the addition of homopolymer containing repeat units that are hydrogen bond donors causes the microphase separation of PPO from the phase containing PEO and the homopolymer, resulting in formation of well-ordered morphologies.[6,7,25] It was found that favorable enthalpic interactions can offset the entropic penalties associated with the incorporation of large homopolymers that results in macrophase separation in weakly interacting BCP−homopolymer blends.[43−45] Supercritical CO_2 assisted infusion of silica precursors into thin film templates comprised of these blends followed by calcination resulted in the formation of well-ordered mesoporous silica films.[24,25]

Hydrogen bond interactions have recently attracted a great deal of attention as a tool for manipulating polymer self-assembly as they can be utilized quite generally due to many available choices of complementary donor−acceptor functionalities. For example, the addition of small molecules such as 3-*n*-pentadecylphenol to BCPs containing polyvinylpyridine (PVP) blocks forms hydrogen bond-assisted supramolecular assemblies that show a rich phase behavior.[46,47] The alkyl chain can microphase separate to form its own domains within the BCP domains allowing formation of new hierarchical structures.[10,48,49] In contrast, we recently showed that small molecules with non-interacting aromatic cores functionalized around their periphery with multiple carboxylic acid or phenol groups can form hydrogen bonds to the PEO blocks of disordered Pluronic BCPs (poly(ethylene oxide)−poly(propylene oxide)−poly(ethylene oxide)) to induce microphase segregation, resulting in the formation of well-ordered morphologies.[5] The presence of the peripheral functional groups "shielded" the aromatic core from unfavorable interactions with the host domain. Uniform functionalization around the periphery of the additives provides favorable interactions with the target block, resulting in high additive loadings within spherical, cylindrical, or lamellar domains without the formation of new hierarchical structures. When the additives are small with respect to the domain size, uniformity in the functionalization can also give rise to uniformity in physicochemical properties within a domain, which is important for many applications such as block copolymer lithography.[12,50] We recently extended this concept to nanoparticles functionalized with hydrogen bond donating ligands to yield well-ordered hybrid materials with high additive loadings.[51]

In this work, we show that hydrogen bond interactions between functionalized polyhedral oligomeric silsesquioxanes (POSS) cages and one segment of a block copolymer can yield well ordered composites with POSS concentrations of up to 80% by mass. More specifically we use POSS cages bearing maleamic acid or aminophenyl groups on each Si atom as the as hydrogen bond donors and PEO segments of Pluronic triblock copolymer surfactants (PEO−PPO−PEO) or polystyrene-poly(ethylene oxide) (PS−PEO) BCPs as the hydrogen bond acceptor (Scheme 1).

Scheme 1. Disorder-to-Order Transitions of Poly(ethylene oxide) Containing Block Copolymers Induced by Blending of Polyhedral Oligomeric Silsesquioxanes Functionalized with Maleamic Acid or Aminophenyl Groups[a]

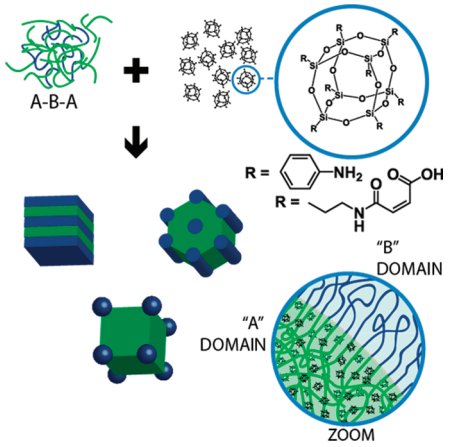

[a] Strong and selective hydrogen bonding interaction of the additives with the poly(ethylene oxide) block (green chains) results in microphase segregation of the PPO blocks (blue chains) to form well ordered BCP composites in which the additives are sequestered into the PEO (green) phase.

The choice of POSS as the additive core is useful for a variety of applications. In general, high loadings of well-dispersed rigid nanofillers are important to mechanical reinforcing of polymers and POSS is often used for this purpose. In addition, POSS cages sequestered within an organic matrix can condense to form silica upon calcination.[52] We utilize this attribute to produce well-ordered mesoporous silica directly from the POSS composites described here. High loadings of POSS in the PEO phase correspond to high silica precursor loadings, which is expected to facilitate preservation of the composite morphology throughout the calcination process. In other areas, self-assembled BCP templates with etch resistant POSS cages chemically grafted to one of the block were demonstrated to be useful in block copolymer lithography.[12] A strategy of simply blending the POSS cages into the BCP using the approaches described here rather than chemical grafting is advantageous in terms of synthetic simplicity and versatility.

EXPERIMENTAL SECTION

Materials. Commercially available commodity surfactant, Pluronic triblock copolymers F108 (PEO_{127}−PPO_{48}−PEO_{127}, 14.6 kg mol^{-1}), F88 (PEO_{109}-PPO_{41}−PEO_{109}, 11.4 kg mol^{-1}), and F68 (PEO_{82}−PPO_{31}−PEO_{82}, 8.4 kg mol^{-1}) each containing about 80% PEO and P105 (PEO_{34}−PPO_{52}−PEO_{34}, 6.5 kg mol^{-1}) containing 50% PEO were donated by BASF. Pluronic surfactants are known to be contaminated with diblock impurities and using gel permeation chromatography their polydispersity indices (PDIs) were found to be in the range of 1.18 to 1.25. Polystyrene−poly(ethylene oxide) (PS−PEO) of molecular weight 3.8 kg/mol (PS) to 4.8 kg/mol (PEO) and a PDI of 1.05 was purchased from Polymer Source. Polyhedral oligomeric silsesquioxane (POSS) octamaleamic acid (POSS−OAA, M_w= 1592 g mol^{-1}) and octaaminophenyl POSS (POSS−OAP, M_w= 1154 g mol^{-1}) were

purchased from Hybrid Plastics. *N,N*-Dimethylformamide (DMF) was purchased from Fisher Scientific. All the materials were used as received.

Sample Preparation. To known masses of the Pluronic BCPs and additives (POSS−OAA or POSS−OAP) was added sufficient DMF to make 10% solids concentration. These samples were heated to 65 °C for 2 h and with occasional stirring to form homogeneous solutions. The solutions were then drop casted on glass slides and kept at 75 °C for 24 to 36 h in a vacuum oven during which drying and annealing occurred. The same protocol was employed for preparation of neat F108 and neat additive samples. Solvent mass losses were tracked during the drying process to confirm that the resulting samples did not contain any residual solvent. The samples made with PS−PEO BCP were also dissolved in DMF, followed by drying at 75 °C for 6 h. Following this, they were annealed at 100 °C for 30 h in a vacuum oven. In this work, compositions are reported as mass ratios of additive to F108. For example, a blend referred to as 30/70 (or 30% loading) contains 30% additive and 70% F108 by mass.

Small-Angle X-ray Scattering (SAXS). The dried samples were placed in the center of 1 mm thick metal washers. Sufficient sample was added to fill the washers completely and the washers were sealed on both sides with kapton film. The filled metal washers were put in metal cells that fit on a vertical heater installed inside the sample chamber and heated to 80 °C. SAXS was performed using a custom instrument from Molecular Metrology Inc. (presently sold as Rigaku S-Max3000). It uses a 30 W microsource (Bede) with a 30 × 30 μm^2 spot size matched to a Maxflux optical system (Osmic) leading to a low-divergence beam of monochromatic Cu Kα radiation (wavelength λ=0.1542 nm). The beam size as it impinges on the sample is 0.4 mm diameter. A two-dimensional gas-filled wire detector was used for collection of scattered X-rays. The whole system was evacuated during operation and a 30 min temperature equilibration time at 80 °C was employed before each measurement. The sample to detector distance was calibrated using silver behenate standard peak at 1.076 nm^{-1}. This allows measurements in wave vector (q) range of $0.06 < q < 1.6$ nm^{-1} in which $q = (4\pi/\lambda) \sin\theta$, where 2θ is the scattering angle. The raw scattering data was circularly averaged and plotted as intensity vs q where intensity was used in arbitrary units as the scattering profiles were shifted vertically for clarity in data presentation. The d-spacing calculated as $d = 2\pi/q^*$ ($q^* = q$ position of the primary peak) provides an estimate of the interplanar spacing between 100 and 110 planes for hexagonally packed cylindrical morphology and body centered cubic packed spherical morphology, respectively.

Differential Scanning Calorimetry (DSC). DSC was carried out to confirm the blending of additives and the nature of their interaction with PEO phase of F108. The blends prepared for SAXS were used for DSC to obtain a complementary set of results. Sample mass of 10 to 15 mg were filled in hermetically sealed aluminum pans. DSC was performed using a TA Instruments Q100 DSC equipped with an RCS cooling system under nitrogen gas purge with a flow rate of 50 mL min^{-1}. All measurements were conducted in the temperature range of −90 to +80 °C at a constant heating and cooling rate of 10 °C min^{-1} under nitrogen atmosphere with a 2 min isothermal hold at both extremes in temperature. The thermograms shown were obtained in the second heating cycle to maintain the same thermal history through all the samples. The temperature calibration was carried out using indium as a standard (T_m = 156.6 °C) and the indium heat of fusion (28.6 J g^{-1}) was used to calibrate the heat flow. For clarity in data presentation, the thermograms obtained were shifted vertically with respect to the thermogram for F108 which is reported as obtained.

X-ray Diffraction (XRD). The samples were heated overnight at 80 °C in a vacuum oven and then were kept at room temperature for about 30 to 45 min before XRD was performed. The XRD was performed in the 2θ range of 5 to 35 degrees at room temperature using a PANalytical X-ray diffraction system using a divergence slit of $^1/_{16}$ in. and an X'Celerator detector. The data obtained were shifted vertically for clarity in data presentation.

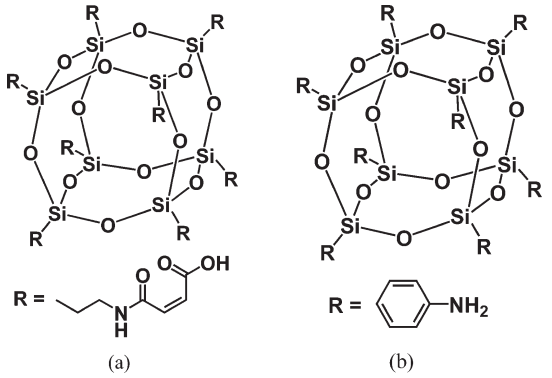

Figure 1. Structure of additives incorporated into Hydrogen bond-donating additives incorporated into the PEO phase of F108: (a) POSS octamaleamic acid (POSS−OAA, M_w = 1592 g mol^{-1}) (b) octaaminophenyl POSS (POSS−OAP, M_w = 1154 g mol^{-1}).

Procedure for the Preparation of Mesoporous Silica. The 50% and 70% blends of POSS−OAA and F108 were casted from their DMF solution under vacuum at 80 °C. After 24 h of vacuum drying and annealing, while maintaining the samples under vacuum, the temperature was raised slowly to 120 °C at a rate of 2 °C every half hour and then maintained at 120 °C for about 10 h. Following this, the temperature was raised to 135 °C at a rate of 2 °C every half hour and maintained for 10 h. The temperature was then raised to 160 at 2 °C every half hour and maintained for 6 h. The samples were then cooled down to room temperature in a period of 3 h. These samples were then calcined in the presence of air by ramping up the temperature to 650 °C at a rate of 1 °C/min and then maintaining at 650 °C for 8 h followed by cooling down to room temperature at a rate of 1 °C/min. White mesoporous silica was obtained and characterized using transmission electron microscopy.

Transmission Electron Microscopy (TEM). The mesoporous silica samples obtained after calcination were ground to a fine powder and suspended in ethanol. Carbon coated copper grids were dipped into the suspensions to collect the particles on the grid. Ethanol was dried off the grid and TEM was performed using a JEOL 100CX transmission electron microscope operated at 100 kV. No staining of the samples was performed.

Fourier Transform Infrared Spectroscopy (FTIR). FTIR was performed using Perkin-Elmer 100 infrared spectrometer. Spectra were obtained from 4000 to 400 cm^{-1}, and were averaged over 32 scans with a 2 cm^{-1} resolution. For these measurements, the samples were crushed and placed directly on the diamond crystal and pressed on top for appropriate contact with the crystal. The spectra obtained were shifted vertically for clarity in data presentation.

RESULTS AND DISCUSSION

The structures of POSS−OAA and POSS−OAP are shown in Figure 1. We compare the two additives in terms of their interactions with the PEO chains, the corresponding phase behavior of their blends, and the morphologies obtained. We express loadings in terms of mass percent of the additive. It should be noted that because the mass of the ligands on POSS−OAA is larger than that of the ligands on POSS−OAP, the POSS cage loading in the PEO phase on a ligand free basis is greater for the POSS−OAP blends at equivalent additive loadings.

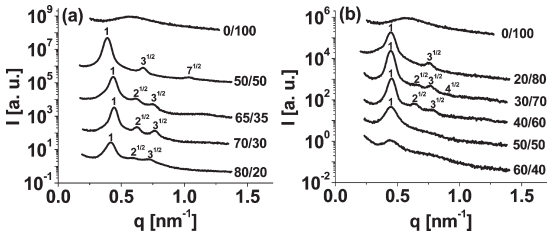

Figure 2. SAXS profiles of neat F108 and its blends with (a) POSS−OAA and (b) POSS−OAP at varying compositions of the blend at 80 °C.

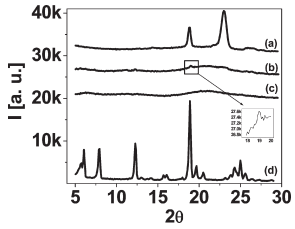

Figure 3. X-ray diffraction profiles of (a) neat F108, (b) 50% loading of POSS−OAA with F108, (c) 70% loading of POSS−OAA with F108, and (d) neat POSS−OAA.

We first present the phase behavior of these additives with F108. Figure 2a shows the SAXS profiles of the blends of POSS−OAA and F108 collected at 80 °C to avoid complications from PEO crystallization. While the neat F108 shows a correlation hole peak that is a characteristic signature of disordered BCPs,[3] incorporation of POSS−OAA induced microphase segregation to form well-ordered morphologies as indicated by sharpening of the primary peak and presence of multiple higher order reflections. In this system, PPO forms the minority phase and PEO + POSS−OAA form the matrix. Selective incorporation of POSS−OAA in the PEO rich domain is confirmed by XRD, DSC and TEM characterization as discussed later. At 50% loading of POSS−OAA, a blend with well-ordered hexagonally packed cylindrical morphology was obtained with a *d*-spacing ($=2\pi/q^*$) of ∼16 nm. At 65% loading the structure of the blend transitioned into a well-ordered body centered cubic spherical morphology with a *d*-spacing of 14.5 nm. This transition from cylindrical to spherical morphology also indicates the selective incorporation of POSS−OAA in the PEO phase which causes the volume fraction of PPO phase to decrease. The spherical morphology persisted at 70% loading but at 80% loading, the peaks began to broaden implying a weakening of positional correlation of PPO domains. These samples were found to be optically clear at all compositions and the SAXS profiles varied systematically as a function of composition indicating that macrophase separation of POSS−OAA from F108 did not occur.

Since the incorporation of POSS and the consequent ordering of F108 is directly dependent on the interaction of the functional groups on the POSS cages with PEO, we next explored the effect of a change in functional groups on POSS cages from maleamic acid to aminophenyl on the phase behavior. As shown in Figure 2b, at 20% loading, POSS−OAP forms a cylindrical morphology with F108 with a *d*-spacing of ∼14 nm. A transition from cylindrical to spherical morphology occurs between 20% and 30% loading. The spherical morphology persists until 40% loading. The SAXS profile indicates a broadening of the primary peak and disappearance of the higher order reflections indicating a loss in positional correlation of PPO domains at 50% loading of POSS−OAP in the composite blend. The systematic variation of the SAXS profile as the composition is increased again suggests that these high additive loadings are achieved without macrophase segregation. We note here that the SAXS profiles (data not shown) of neat POSS−OAA or POSS−OAP are featureless, indicating that these additives do not form nanoscale structures on their own. However, as discussed later, the additives can crystallize on their own however the lattice spacings are outside the range that can be captured using the present SAXS set up.

To convert the mass percentages cited above into volume percentages (a more thermodynamically relevant parameter) the liquid-like (amorphous) densities of POSS−OAA and POSS−OAP are required, but they are not reported as these materials decompose below their melting points. Therefore, a precise conversion of mass percent to volume percent is not possible. However, the POSS cages functionalized with other ligands (for example short alkane chains with terminal epoxy groups) are liquids with density in the range of 1.2 to 1.25 g/cm^3. It is expected that the liquid-like densities of POSS−OAA and POSS−OAP would fall in a similar range. Since F108 melt has a density nearly equal to 1 g/cm^3, the POSS volume fractions are expected to be slightly smaller than the mass fractions reported here. For example, 80 mass % POSS−OAA in a blend would correspond to about 77 vol %.

The mass of the POSS cage is 26.2% of the entire POSS−OAA molecule and therefore a loading of 80% POSS−OAA translates to 21% loading of the inorganic cores. The formation of such highly loaded and well-ordered composites is promising because it shows how suitable chemical functionalities can lead to high levels of incorporation of additives. It is also interesting to find that just a little F108 can guide the spatial assembly of a large quantity of POSS−OAA while maintaining the block copolymer morphology. This is a particularly interesting finding in light of the literature, which suggests that the entropic penalty associated with polymer chain stretching around the additives tends to cause macrophase separation of the additive from the polymer and thus sets a limit to the maximum loading.[34] The strong interaction between the additive and block copolymer also serve to suppress additive aggregation. Additive aggregation is not only often undesirable in terms of materials properties, but large aggregates can also disrupt the BCP structure.[53] The mass of the POSS cage in the POSS−OAP additive is 36.2% and therefore a 40% loading of POSS−OAP corresponds to 14.5% loading of POSS cores. Thus, maleamic acid ligands lead to higher POSS loadings as compared to aminophenyl ligands while maintaining a well-ordered BCP morphology. It is interesting to note that the concentration of POSS−OAA and POSS−OAP in the POSS-loaded PEO phase of the ordered composite can be as high as about 80% and 40% by volume, respectively. This is in contrast to the other BCP-additive systems in which the BCP chains are the major component.

Blends of POSS−OAA with other Pluronic BCPs of lower molecular weight resulted in the formation of composites with smaller *d*-spacings and a lamellar morphology was accessible using a nearly symmetric Pluronic BCP (see Supporting Information). To test the generality of this additive-driven assembly of PEO containing BCPs, the ability to incorporate POSS−OAA into a PS−PEO block copolymer was also determined and it was found that a POSS−OAA induced phase segregation in

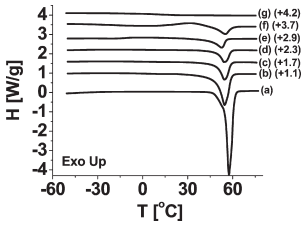

Figure 4. DSC thermograms of neat F108 and its blend with POSS−OAA and POSS−OAP: (a) neat F108, (b) 20/80 POSS−OAP/F108, (c) 30/70 POSS−OAP/F108, (d) 40/60 POSS−OAP/F108, (e) 50/50 POSS−OAP/F108, (f) 50/50 POSS−OAA/F108, and (g) 70/30 POSS−OAA/F108. The constants added to the heat flow values to shift the blend thermograms vertically upward are shown in parentheses.

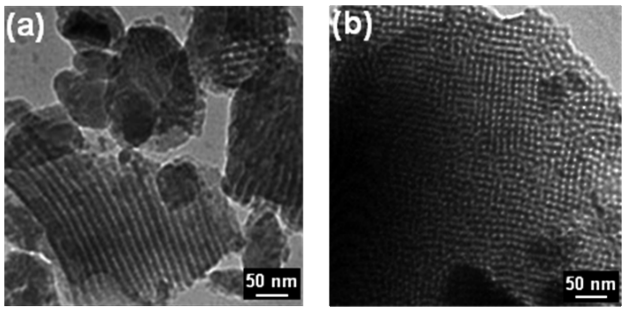

Figure 5. Transmission electron micrographs of mesoporous silica obtained upon calcination of F108 composites containing (a) 50% POSS−OAA and (b) 70% POSS−OAA.

Table 1. Thermal Characteristics of Neat F108 and Its Blends with POSS−OAA and POSS−OAP at Varying Compositions

sample	melting temperature [°C]	normalized melting enthalpy [J (g PEO)$^{-1}$]
F108	57.5	162.3
20% POSS−OAP	54.6	123.0
30% POSS−OAP	54.4	75.2
40% POSS−OAP	54.1	60.9
50% POSS−OAP	52.7	60.7
50% POSS−OAA	55.0	47.3
70% POSS−OAA[a]	-	-

[a] 70% POSS−OAA blend did not show any melting indicating inhibition of PEO crystallization.

an otherwise disordered low molecular weight PS−PEO BCP (see Supporting Information).

The molecular mixing of POSS−OAA with PEO phase of F108 was confirmed using XRD at high angles. Figure 3 compares the XRD profiles of neat F108 and neat POSS−OAA with blends of F108 and POSS−OAA at 50% and 70% loading. Neat F108 shows a crystalline structure due to formation of PEO crystallites[54] and neat POSS−OAA shows multiple peaks indicating that it also crystallizes. Upon blending POSS−OAA and F108, the peaks corresponding to neat POSS−OAA disappeared completely, indicating molecular dispersion of POSS−OAA in the PEO phase. At 50% loading, the intensity of the peaks corresponding to PEO crystallites of neat F108 diminishes significantly in intensity although a low intensity peak is still visible at a 2θ value of ~18. The peaks disappear completely at 70% loading indicating complete inhibition of crystallization of PEO. This implies good mixing such that PEO and POSS−OAA inhibit each other's crystallization and prefer to associate by hydrogen bonding instead of self-association by means of crystallization. These results of slight crystallanity of PEO at 50% loading while total inhibition of crystallanity at 70% loading is consistent with the DSC results discussed next.

DSC was performed to further explore the nature of interaction of the two additives with the PEO chain segments and to assess their compatibility as done previously.[5,25] Figure 4 shows the DSC thermograms of neat F108 and its blend with POSS−OAA and POSS−OAP at temperatures between −60 and +75 °C. For clarity in data presentation, the thermograms for the blends were shifted vertically upward by adding constant values to heat flow as given in parentheses beside each thermogram. The melting endotherms observed correspond to the melting of the PEO crystallites (PPO does not crystallize). The corresponding melting temperatures, denoted by the peak position of the endotherm, and the melting enthalpy normalized by the fraction of PEO present in the blends are tabulated in Table 1. Upon incorporation of POSS−OAA and POSS−OAP, the melting temperature and the normalized melting enthalpy decrease, which is consistent with the favorable interaction of these additives with the PEO chain segments. At 70% POSS−OAA loading, the crystallization of PEO was completely inhibited and no melting endotherm was observed. While the systematic variation of the DSC thermograms obtained is consistent with compatibility of both additives with PEO, POSS−OAA causes larger reductions in the normalized melting enthalpy than POSS−OAP, which implies that the interaction of POSS−OAA with PEO is stronger than that of POSS−OAP. This is also consistent with higher loadings possible for POSS−OAA than POSS−OAP in the composites as seen in the phase behavior characterizations.

It is known that POSS cages can be oxidized into a silica network upon calcination.[52,55] However, the cages must be sequestered within an organic matrix to prevent their volatilization before they begin to cross-link.[55,56] Additionally, a high composition of POSS cages is desired so that they are situated in close proximity for mutual condensation. Since POSS−OAA can be incorporated selectively into the PEO phase of F108 at high loadings, the close proximity of cages is ensured. The maleamic acid groups bear carboxylic acid and secondary amine groups which can be cross-linked by heating to 160 °C by the formation of imides and formation of anhydrides.[57] Blends of F108 with 50% or 70% POSS−OAA were heated by gradually raising the temperature to 160 °C, which was found to be sufficient to form a cross-linked network of POSS−OAA within the PEO phase. This thermal treatment caused the blends to transform from a sticky paste to a flexible self-supporting nonsticky and insoluble solid indicating qualitatively that cross-linking occurred. FTIR measurements discussed below were used to track the reactions that occurred at different stages of the processing for the F108 composite. The cross-linked samples were then placed in a calcination oven where, in the presence of air, the temperature was gradually raised to 650 °C over a period of 10 h, maintained at 650 °C for 8 h and then ramped down to room temperature over a period of 10 h. During calcinations, the yellow colored cross-linked samples were converted to white mesoporous silica powder and flakes, which were then characterized by TEM. Figure 5 shows the TEM micrographs obtained for the mesoporous silica obtained from the two blends, which confirm

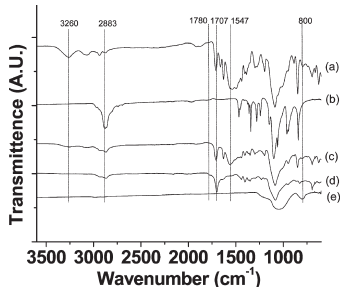

Figure 6. FTIR spectra: (a) neat POSS−OAA, (b) neat F108, (c) 70% POSS−OAA/F108 blend annealed to 75 °C, (d) 70% POSS−OAA/F108 blend annealed to 160 °C, and (e) 70% POSS−OAA/F108 blend calcined to 650 °C.

that the cylindrical and spherical morphologies of the original blends were preserved upon calcination.

In previous work,[25] FTIR was utilized to demonstrate hydrogen bonding between the carboxylic acid groups of poly(acrylic acid) with the ether oxygen of PEO. On similar lines, here FTIR spectra were obtained for the 70% POSS−OAA/F108 blend after vacuum drying at 75 °C and after annealing at 160 °C as shown in Figure 6. For comparison, the spectra of neat F108 and neat POSS−OAA are also shown. Changes in the spectra obtained at 75 and 160 °C indicate reaction of carboxylic acid groups with the secondary amine groups as is known to occur in similar systems.[58,59] Carboxylic acid groups can also react among themselves to form anhydrides. The peaks between 3420 and 2775 cm^{-1} in the spectrum of 70% POSS−OAA/F108 blend after annealing at 75 °C, match exactly in their positions with the peaks in this region for the case of neat POSS−OAA. More specifically, the peaks at 3261 and 3072 cm^{-1} can be attributed to the presence of secondary amine and hydroxyl groups on carboxylic acid, respectively. However, both these peaks disappear after annealing at 160 °C indicating imide formation by reaction between carboxylic acid groups and the secondary amine groups. The appearance of a peak at 1780 cm^{-1} corresponds to carbonyl group of the imide formed.[60] Additionally, the disappearance of the N−H stretching peak at 3261 cm^{-1}, and the secondary N−H bending peak at 1560 cm^{-1}, also confirms the cross-linking between the secondary amine and the carboxylic acid groups. The peak at 1707 cm^{-1} contributed from POSS−OAA can be attributed to the carbonyl groups of the carboxylic acid. This peak shifts to 1700 cm^{-1} upon annealing to 160 °C, and might be linked to a change in the response of carbonyl group upon reaction of carboxylic acid groups. FTIR spectrum of the mesoporous silica formed from the 70% POSS−OAA/F108 blend was also obtained to explore the changes upon calcination to 650 °C. Most peaks corresponding to the organic components disappear which implies that most organic material was removed upon calcinations, which is expected at high calcination temperatures. The broad hump between 1100 and 1000 cm^{-1} and the shoulder around 1210 cm^{-1} correspond to the stretching Si−O−Si bonds.[61] The peak at 800 cm^{-1} indicates the formation of Si−C, which could form as the first carbon on the ligand is covalently bound to the Si on the POSS cage.[62] The presence of some carbonaceous material is indicated by the CH_2 and CH_3 stretching peaks around 3000 cm^{-1} which could arise from some trapping of impurities during the calcinations process.[62]

Pluronic surfactants have been used widely as structure directing agents with TEOS precursors via cooperative assembly from solution in which structural evolution and silica network condensation occur simultaneously.[63,64] One important difference/advantage of the method shown in this work is that structural evolution and silica network formation occur as distinct steps which enables facile handling and processing of the composite material prior to network formation, which has additional advantages for controlling the ultimate architecture of the material. Furthermore, the precursor-loaded composites are formed under conditions at which the silica precursor is stable, which is not the case in traditional approaches. The use of a stable intermediate material eliminates much of the process dependent variability in materials prepared using complex interactions and reactions in solution which are quite sensitive to pH, evaporation rate, aging time, solvent, and temperature.

CONCLUSIONS

POSS cages fully functionalized with maleamic acid or aminophenyl ligands capable of hydrogen bonding with the PEO blocks of low molecular weight BCPs can induce order in the otherwise disordered BCP melts, producing well-ordered and highly filled composites with small domains. The phase behavior of the composites depends significantly upon the choice of hydrogen bonding ligands, however, blends with both additives with F108 formed well-ordered cylindrical and spherical morphologies. Lamellar morphologies were accessible using Pluronic P105 as the template. Between the two ligands, maleamic acid was found to result in higher levels of incorporation than aminophenyl while maintaining the well-ordered BCP morphology. Strong order in the BCP nanostructure was maintained up to 80% loading of POSS−OAA and up to 40% loading of POSS−OAP in F108. In comparison to POSS−OAP, POSS−OAA interacts more strongly with PEO which allows higher levels of incorporation. XRD and DSC measurements indicated miscibility and compatibility of both the additives with PEO. The concept of using hydrogen bond interactions to enable the formation or well ordered BCP−additive composites appears to be general and can be applied to other systems.

Cross-linking of the POSS−OAA−F108 composite at 50% and 70% additive loadings upon heating to 160 °C followed by calcination at 650 °C yielded mesoporous silica with cylindrical and spherical morphologies that were templated by the presence of the BCP. This is consistent with phase selective incorporation of the POSS additives into the PEO phase.

ASSOCIATED CONTENT

Supporting Information. SAXS profiles for blends of POSS−OAA with various other Pluronic BCPs and with a PS−PEO BCP. This material is available free of charge via the Internet at http://pubs.acs.org.

AUTHOR INFORMATION

Corresponding Author

*E-mail: watkins@polysci.umass.edu.

ACKNOWLEDGMENT

This work was supported by the NSF Center for Hierarchical Manufacturing at the University of Massachusetts (CMMI-0531171). The schematic shown Scheme 1 was made by Alexander Niemeyer.

REFERENCES

(1) Bockstaller, M. R.; Mickiewicz, R. A.; Thomas, E. L. *Adv. Mater.* **2005**, *17* (11), 1331–1349.

(2) Bates, F. S.; Fredrickson, G. H. *Phys. Today* **1999**, *52* (2), 32–38.

(3) Leibler, L. *Macromolecules* **1980**, *13* (6), 1602–1617.

(4) Bates, F. S.; Fredrickson, G. H. *Annu. Rev. Phys. Chem.* **1990**, *41*, 525–57.

(5) Daga, V. K.; Watkins, J. J. *Macromolecules* **2010**, *43* (23), 9990–9997.

(6) Tirumala, V. R.; Daga, V.; Bosse, A. W.; Romang, A.; Ilavsky, J.; Lin, E. K.; Watkins, J. J. *Macromolecules* **2008**, *41* (21), 7978–7985.

(7) Tirumala, V. R.; Romang, A.; Agarwal, S.; Lin, E. K.; Watkins, J. J. *Adv. Mater.* **2008**, *20* (9), 1603–1608.

(8) Misner, M. J.; Skaff, H.; Emrick, T.; Russell, T. P. *Adv. Mater.* **2003**, *15* (3), 221–224.

(9) Sohn, B. H.; Cohen, R. E. *Acta Polym.* **1996**, *47* (8), 340–343.

(10) van Zoelen, W.; ten Brinke, G. *Soft Matter* **2009**, *5* (8), 1568–1582.

(11) Bondzic, S.; de Wit, J.; Polushkin, E.; Schouten, A. J.; ten Brinke, G.; Ruokolainen, J.; Ikkala, O.; Dolbnya, I.; Bras, W. *Macromolecules* **2004**, *37* (25), 9517–9524.

(12) Hirai, T.; Leolukman, M.; Liu, C. C.; Han, E.; Kim, Y. J.; Ishida, Y.; Hayakawa, T.; Kakimoto, M.; Nealey, P. F.; Gopalan, P. *Adv. Mater.* **2009**, *21* (43), 4334–4338.

(13) La, Y. H.; Park, S. M.; Meagley, R. P.; Leolukman, M.; Gopalan, P.; Nealey, P. F. *J. Vac. Sci. Technol. B* **2007**, *25* (6), 2508–2513.

(14) Park, S.; Lee, D. H.; Xu, J.; Kim, B.; Hong, S. W.; Jeong, U.; Xu, T.; Russell, T. P. *Science* **2009**, *323* (5917), 1030–1033.

(15) Ruiz, R.; Kang, H. M.; Detcheverry, F. A.; Dobisz, E.; Kercher, D. S.; Albrecht, T. R.; de Pablo, J. J.; Nealey, P. F. *Science* **2008**, *321* (5891), 936–939.

(16) Bita, I.; Yang, J. K. W.; Jung, Y. S.; Ross, C. A.; Thomas, E. L.; Berggren, K. K. *Science* **2008**, *321* (5891), 939–943.

(17) Kim, H. C.; Park, S. M.; Hinsberg, W. D. *Chem. Rev. 110* (1), 146−177.

(18) Barber, R. P.; Gomez, R. D.; Herman, W. N.; Romero, D. B. *Org. Electron.* **2006**, *7* (6), 508–513.

(19) Barrau, S.; Heiser, T.; Richard, F.; Brochon, C.; Ngov, C.; van de Wetering, K.; Hadziioannou, G.; Anokhin, D. V.; Ivanov, D. A. *Macromolecules* **2008**, *41* (7), 2701–2710.

(20) Yang, C.; Lee, J. K.; Heeger, A. J.; Wudl, F. *J. Mater. Chem.* **2009**, *19* (30), 5416–5423.

(21) Fink, Y.; Urbas, A. M.; Bawendi, M. G.; Joannopoulos, J. D.; Thomas, E. L. In *Block copolymers as photonic bandgap materials*; Workshop on Electromagnetic Crystal Structures, Laguna Beach, California, Jan 04−06, 1999; Ieee-Inst Electrical Electronics Engineers Inc.: Laguna Beach, CA, 1999; pp 1963−1969.

(22) Urbas, A.; Sharp, R.; Fink, Y.; Thomas, E. L.; Xenidou, M.; Fetters, L. J. *Adv. Mater.* **2000**, *12* (11), 812–814.

(23) Urbas, A.; Fink, Y.; Thomas, E. L. *Macromolecules* **1999**, *32* (14), 4748–4750.

(24) Pai, R. A.; Humayun, R.; Schulberg, M. T.; Sengupta, A.; Sun, J. N.; Watkins, J. J. *Science* **2004**, *303* (5657), 507–510.

(25) Tirumala, V. R.; Pai, R. A.; Agarwal, S.; Testa, J. J.; Bhatnagar, G.; Romang, A. H.; Chandler, C.; Gorman, B. P.; Jones, R. L.; Lin, E. K.; Watkins, J. J. *Chem. Mater.* **2007**, *19*, 5868–5874.

(26) Nagarajan, S.; Li, M. Q.; Pai, R. A.; Bosworth, J. K.; Busch, P.; Smilgies, D. M.; Ober, C. K.; Russell, T. P.; Watkins, J. J. *Adv. Mater.* **2008**, *20* (2), 246–251.

(27) Hillmyer, M. A. Nanoporous materials from block copolymer precursors. In *Block Copolymers II*; Springer-Verlag: Berlin, 2005; Vol. 190, pp 137−181.

(28) Kang, M.; Moon, B. *Macromolecules* **2009**, *42* (1), 455–458.

(29) Luchnikov, V.; Kondyurin, A.; Formanek, P.; Lichte, H.; Stamm, M. *Nano Lett.* **2007**, *7* (12), 3628–3632.

(30) Park, S. C.; Kim, B. J.; Hawker, C. J.; Kramer, E. J.; Bang, J.; Ha, J. S. *Macromolecules* **2007**, *40* (22), 8119–8124.

(31) Jeong, U.; Ryu, D. Y.; Kho, D. H.; Kim, J. K.; Goldbach, J. T.; Kim, D. H.; Russell, T. P. *Adv. Mater.* **2004**, *16* (6), 533–536.

(32) Lin, Y.; Boker, A.; He, J. B.; Sill, K.; Xiang, H. Q.; Abetz, C.; Li, X. F.; Wang, J.; Emrick, T.; Long, S.; Wang, Q.; Balazs, A.; Russell, T. P. *Nature* **2005**, *434* (7029), 55–59.

(33) Wang, J. Y.; Chen, W.; Sievert, J. D.; Russell, T. P. *Langmuir* **2008**, *24* (7), 3545–3550.

(34) Balazs, A. C.; Emrick, T.; Russell, T. P. *Science* **2006**, *314* (5802), 1107–1110.

(35) Warren, S. C.; Messina, L. C.; Slaughter, L. S.; Kamperman, M.; Zhou, Q.; Gruner, S. M.; DiSalvo, F. J.; Wiesner, U. *Science* **2008**, *320* (5884), 1748–1752.

(36) Mayes, A. M.; Delacruz, M. O. *J. Chem. Phys.* **1989**, *91* (11), 7228–7235.

(37) Matsen, M. W.; Thompson, R. B. *J. Chem. Phys.* **1999**, *111* (15), 7139–7146.

(38) Ruzette, A. V. G.; Soo, P. P.; Sadoway, D. R.; Mayes, A. M. *J. Electrochem. Soc.* **2001**, *148* (6), A537–A543.

(39) Chen, J.; Frisbie, C. D.; Bates, F. S. *J. Phys. Chem. C* **2009**, *113* (10), 3903–3908.

(40) Epps, T. H.; Bailey, T. S.; Pham, H. D.; Bates, F. S. *Chem. Mater.* **2002**, *14* (4), 1706–1714.

(41) Epps, T. H.; Bailey, T. S.; Waletzko, R.; Bates, F. S. *Macromolecules* **2003**, *36* (8), 2873–2881.

(42) Kim, S. H.; Misner, M. J.; Yang, L.; Gang, O.; Ocko, B. M.; Russell, T. P. *Macromolecules* **2006**, *39* (24), 8473–8479.

(43) Hashimoto, T.; Tanaka, H.; Hasegawa, H. *Macromolecules* **1990**, *23* (20), 4378–4386.

(44) Tanaka, H.; Hasegawa, H.; Hashimoto, T. *Macromolecules* **1991**, *24* (1), 240–251.

(45) Lowenhaupt, B.; Steurer, A.; Hellmann, G. P.; Gallot, Y. *Macromolecules* **1994**, *27* (4), 908–916.

(46) Tung, S. H.; Kalarickal, N. C.; Mays, J. W.; Xu, T. *Macromolecules* **2008**, *41* (17), 6453–6462.

(47) van Zoelen, W.; Asumaa, T.; Ruokolainen, J.; Ikkala, O.; ten Brinke, G. *Macromolecules* **2008**, *41* (9), 3199–3208.

(48) Ruokolainen, J.; Makinen, R.; Torkkeli, M.; Makela, T.; Serimaa, R.; ten Brinke, G.; Ikkala, O. *Science* **1998**, *280* (5363), 557–560.

(49) Ruokolainen, J.; Saariaho, M.; Ikkala, O.; ten Brinke, G.; Thomas, E. L.; Torkkeli, M.; Serimaa, R. *Macromolecules* **1999**, *32* (4), 1152–1158.

(50) Hawker, C. J.; Russell, T. P. *MRS Bull.* **2005**, *30* (12), 952–966.

(51) Lin, Y.; Daga, V. K.; Anderson, E. R.; Gido, S. P.; Watkins, J. J. *J. Am. Chem. Soc.* **2011**, *133* (17), 6513–6516.

(52) Moon, J. H.; Seo, J. S.; Xu, Y. G.; Yang, S. *J. Mater. Chem.* **2009**, *19* (27), 4687–4691.

(53) Zhao, Y.; Hashimoto, T.; Douglas, J. F. *J. Chem. Phys.* **2009**, *130*, 12.

(54) Mihailov, M.; Bogdanov, B.; Davarska, G. *Acta Polym.* **1985**, *36* (9), 481–483.

(55) Fina, A.; Tabuani, D.; Carniato, F.; Frache, A.; Boccaleri, E.; Camino, G. *Thermochim. Acta* **2006**, *440* (1), 36–42.

(56) Mabry, J. M.; Vij, A.; Iacono, S. T.; Viers, B. D. *Angew. Chem., Int. Ed.* **2008**, *47* (22), 4137–4140.

(57) Maurer, J. J.; Eustace, D. J.; Ratcliffe, C. T. *Macromolecules* **1987**, *20* (1), 196–202.

(58) Mehta, N. B.; Phillips, A. P.; Lui, F. F.; Brooks, R. E. *J. Org. Chem.* **1960**, *25* (6), 1012–1015.

(59) Coleman, L. E.; Bork, J. F.; Dunn, H. *J. Org. Chem.* **1959**, *24* (1), 135–136.

(60) Hanes, J.; Chiba, M.; Langer, R. *Macromolecules* **1996**, *29* (16), 5279–5287.

(61) Vasquez-A, M. A.; Rodriguez, G. A.; Garcia-Salgado, G.; Romero-Paredes, G.; Pena-Sierra, R. *Rev. Mex. Fis.* **2007**, *53* (6), 431–435.

(62) Silverstein, R. M.; Webster, F. X.; Kiemle, D. J., *Spectrometric identification of organic compounds*. John Wiley & Sons, Inc.: New York, 2005.

(63) Zhao, D.; Feng, J.; Huo, Q.; Melosh, N.; Fredrickson, G. H.; Chmelka, B. F.; Stucky, G. D. *Science* **1998**, *279* (5350), 548–552.

(64) Wan, Y.; Zhao, D. *Chem. Rev.* **1998**, *107* (7), 2821–2860.